# PHYSICS OF INTERPLANETARY DUST COLLECTION WITH AEROGEL

## Final Report and Summary of Research

NASA Grant NAG-9-913
Johnson Space Center
September 30, 1996-March 31 1998

*William W. Anderson*
*Department of Geology and Physics*
*Georgia Southwestern State University*
*800 Wheatley Street*
*Americus, GA 31709*

*March 31, 1998*

**Summary**

This report presents the results of research undertaken to study various problems associated with hypervelocity capture of dust particles in aerogel. The primary topics investigated were the properties of shocked aerogel and the requirements for reliable capture of particles on the STARDUST mission. In particular, the viscosity of shocked aerogel has been an open question. The results presented here suggest that the viscosity of aerogel at high impact velocities is negligible, although there remains some uncertainty about lower velocities. The model adopted for viscosity treats the mixture of polymeric silica and decomposition products and finds that, for particle velocities of 6-7 km/s, the viscosity is similar to that typical of light gasses at STP. Expressions for the Hugoniot of aerogel as a function of density were also obtained from the available data. All aerogels of interest for cosmic dust collectors have very similar shock velocity-particle velocity Hugoniot curves. The strength behavior of aerogel for low-speed penetration was measured, but further work is needed to study the proper way to apply this to the issue of terminal deceleration of a dust particle. Preliminary calculations designed to maximize the penetration depths were performed to determine the required density of aerogel to reliably stop a particle in a 3 cm thickness of aerogel (the path length expected for a normal impact into the STARDUST collector). In order to stop a particle of density $\rho_p$ and diameter $d_p$, the mean density of the aerogel collector should be no less than that given by the expression $\overline{\rho}_0 = 1.085 \times 10^{-4} \rho_p d_p$, for densities measured in g/cm$^3$ and the particle diameter measured in micrometers.

## INTRODUCTION

This project was undertaken to study the phenomena involved in interplanetary and cometary dust collection by hypervelocity impact into silica aerogel. At the beginning of the project, several important issues were identified: (1) the need to develop a suitable shock Hugoniots and thermal equation of state (EOS) for aerogel; (2) the effects of viscous drag forces on particle deceleration; and (3) heat transfer physics as applied to the present problem. These issues in turn require quantitative knowledge of the penetration strength of aerogel [Anderson et al., 1996] to provide a stopping criterion in numerical models of particle interaction with the aerogel; the sound speed, which affects the penetration speed at which strength becomes important; and the viscosity of silica over the full range of conditions that would be encountered during the impact and deceleration process.

## CONDITIONS IN SHOCKED AEROGEL

In order to properly model the hypervelocity impact of a dust particle into aerogel, we must have suitable descriptions of the shock compression behavior of aerogel and the conditions in the shocked aerogel. In particular, we require a knowledge of the shock Hugoniot curves and the temperature, viscosity, and thermal transport behavior of shocked aerogel.

### Shock Hugoniots.

To characterize the stresses produced during high-velocity impacts of particles into aerogel, we must have a suitable knowledge of the shock Hugoniot of aerogel as a function of the initial density. Relatively few data have been obtained for aerogel [e.g., Holmes et al., 1984; Holmes and See, 1991; Rabie and Dick, 1992; Holmes, 1994], but these can be supplemented with data for low density silica, known as aerosil [Simakov and Trunin, 1990; Vildanov et al., 1996]. At velocities in excess of the longitudinal sound speeds of these materials, there is no reason to expect them to behave differently under shock compression. The Hugoniot curves described by these data are presented in figure 1. At the scale of figure 1, all the Hugoniot curves fall close to one another. Figure 2 shows the curves at an expanded scale. The shock wave velocity, $U_s$, is often expressed as a linear function of the shock state material velocity, $u_p$:

$$U_s = C_0 + su_p$$

where $C_0$ and $s$ are empirical constants. The data, covering a wide range of conditions, suggest a general qualitative model of the aerogel Hugoniot curve that consists of straight line segments, with a slight break in slope occurring in the region $u_p \approx 4$ km/s. The values of $C_0$ and $s$ can be expressed as functions of the initial density $\rho_{00}$, with

$$C_0 = .436 - 2.024\rho_{00} + 4.18\rho_{00}^{\ 2}$$

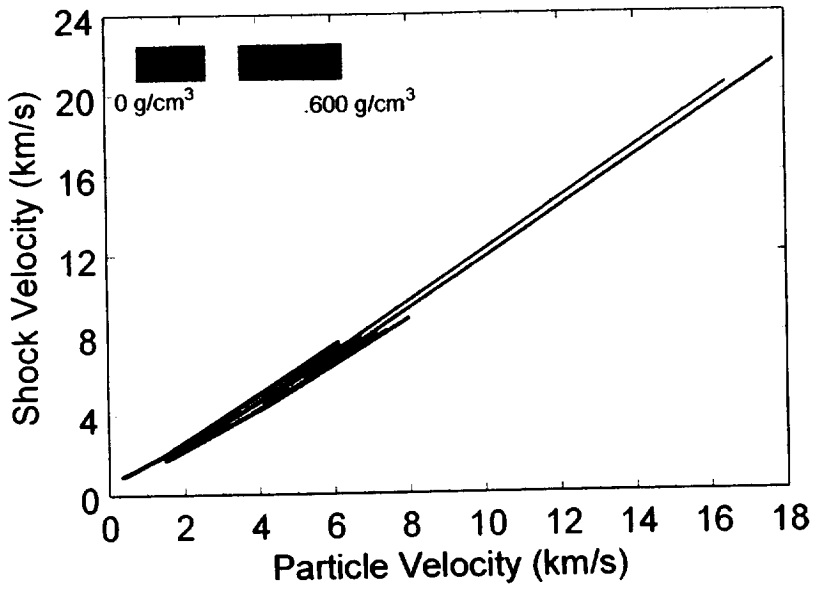


Figure 1. Fit Hugoniots for a range of aerogel densities

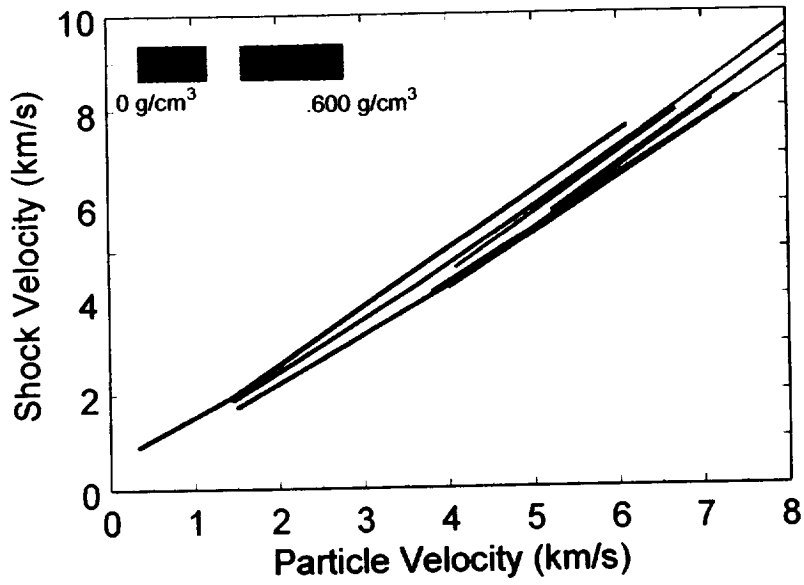


Figure 2. Hugoniots shown in figure 1, at expanded scale.

$$s = 0.700 + 24.4\rho_{00} - 36.3\rho_{00}^{2}$$

at low velocity and

$$C_0 = -0.947 + 1.78\rho_{00}$$

$$s = 1.201 + 0.824\rho_{00}$$

at high velocity, where $C_0$ is expressed in km/s and $\rho_{00}$ is expressed in $Mg/m^3$.

Temperature of Shocked Aerogel.

Examination of $P$-$V$ curves calculated from the $U_s$-$u_p$ relations shows that, just above the break in slope, the density begins to decrease with increasing shock pressure. Both the break in the $U_s$-$u_p$ curve and the occurrence of a density minimum at similar shock conditions is probably the result of bond breakage. This bond breakage should have a significant effect on the temperature and viscosity of the shocked aerogel.

Estimation of the temperature in the shock-compressed state requires us to account for both the bond breakage and the compression process. The total internal energy can be divided into a cold compression part, a thermal part, and a configurational part (which includes the energy that goes into rupturing bonds). For calculating the temperature, we are interested in the thermal part. Usually, the thermal energy is estimated is by subtracting the other components of the energy from the total.

We can approximate the cold compression part of the energy by assuming isentropic compression from STP to the volume of interest, after taking the bond breakage into account. For very porous starting materials, we can usually expect to find that the cold compression energy is relatively small.

Most of the configurational energy change, which we will call the transition energy, $E_{tr}$, consists of energy required to disrupt chemical bonds. In the case of $SiO_2$, the bond strength per mole of $SiO_2$, calculated from the enthalpy of formation and bond strengths of the oxides and elements in their standard states, is 1.943 MJ/mol (32.3 MJ/kg) [Weast, 1975]. This is the decomposition energy. As a crude approximation, the fraction of the Si-O bonds broken is given by

$$x_r \approx e^{-3E_B / E_{th}}$$

where $E_B$ is the bond energy per unit of mass and $E_{th}$ is the thermal part of the specific shock energy. The factor of 3 in the exponential is the result of the three spatial degrees of freedom that enter into the calculation of molar heat capacity. The advantage of casting the bond breakage in this form is that it does not require prior knowledge of the temperature. For the value of $E_{th}$ in an ultralow density material such as aerogel, we can replace $E_{th}$ with the shock-induced increase in total internal energy, $E_H$. The actual amount of reaction $x$ is given by

$$x = x_r e^{-r/t}$$

where $\tau$ is a time constant that is a few times the bond vibration frequency and $t$ is the time available for the reaction. In the case of a bow shock wave in front of an IDP, this is the time required between arrival of the shock wave and the arrival of the front surface of the particle, which we expect to be large compared to the time constant, so we can expect that $x \approx x_r$. The transition energy is then given by

$$E_{tr} = xE_B \approx E_B e^{-3E_B E_H} = E_B e^{-6E_B u_p^2}$$

We can estimate the temperature of shocked aerogel for comparison with experiments by using the equilibrium value of $x$ and assuming that the cold compression energy is negligible. The temperature then is given by

$$T \approx (E_H - E_{tr})/C_V$$

Here, we use the Dulong-Petite limit for the specific heat $C_V$. For aerogel with $\rho_{00} = 0.13$ $Mg/m^3$ for $u_p = 6.56$ km/s, we get $T = 11600$ K, which compares to an experimental value of $10800 \pm 1200$ K [Holmes et al., 1984].

Viscosity of Shocked Aerogel.

Among the more important issues in the deceleration of dust particles in aerogel is the viscosity of the shocked aerogel that flows around the particle. Although no reliable data for the viscosity of $SiO_2$ at the conditions that characterize shocked aerogel exist, only a crude estimate of the viscosity is required. The model developed here accounts for the effects of temperature on the polymeric $SiO_2$ and also for the effects of bond breakage.

The basic model treats shocked aerogel as a mixture of polymeric $SiO_2$ and decomposition products. Since the decomposition products are small molecules, they would, in the absence of the polymeric silica, have a very small viscosity. As long as the volume fraction of the polymer remains high, however, the viscosity also remains high. Qualitatively, as the fraction of bonds broken increases with rising temperature, the viscosity slowly decreases as a result of less connectivity in the polymer and increased thermal motion. At some value of the bond breakage fraction, the polymer is reduced to isolated "globs" of material suspended in a low-viscosity fluid. At this point, the viscosity drops precipitously. As the fraction of bonds broken continues to increase, the viscosity drops slowly until all the polymer has been destroyed. This phenomenology is directly comparable to the effects of partial melting on a material, with the melt fraction at which the viscosity drops rapidly being termed the rheologically critical melt fraction [Arzi, 1978].

In this model, equations describing the viscosity behavior of partially molten systems are adapted to the qualitative description given above in order to provide a quantitative estimate of the viscosity behavior of aerogel as it is shocked to successively greater pressures and temperatures. In particular, we will assume that the viscosity can be described by an appropriately weighted mixing of the viscosities of the two end members—polymeric silica and decomposition products. In order to quantify this description, mathematical expressions are

required for the viscosity of the polymer, the viscosity of the decomposition products, and the mixing scheme for these two end-member viscosities.

*Viscosity of polymeric $SiO_2$.*

A number of data exist on the viscosity of silica glasses at relatively low temperatures (sufficiently low that the amount of decomposition is negligible). One of the more recent studies of the viscosity of silica glasses as a function of temperature is by Weiss [1984]. For the polymeric silica viscosity in the present application, the best model is an Arrhennius-type of viscosity, modified to account for distension. The free-volume approach [Hildebrand, 1971] is not suitable to polymers because of the issues of entanglement of polymeric chains and frameworks. Thus, the distension of the shocked state, relative to the STP density, affects the bulk viscosity of the polymer primarily by introducing voids, which change the viscosity roughly in proportion to the bulk density. Based on the density of fused silica and the results presented by Weiss [1984], the suggested expression for the viscosity of polymeric silica is given by

$$\eta = A\left(\frac{\rho}{\rho_{fq}}\right)e^{E_a\ RT}$$

where $\rho_H$ is the bulk density of the shocked aerogel, $\rho_{fq} = 2.204$ Mg/m$^3$ is the STP density of fused quartz, and $A = 7.11\times10^{-10}$ Pa·s, and $E_a = 6.134\times10^5$ J/mol. It should be noted that, even without accounting for the effects of decomposition, this expression gives very low viscosities at the temperature-volume conditions found in aerogel on the high-velocity portion of the shock Hugoniot. In fact, for the experimental temperature found by Holmes et al. [1984] for $u_p$ = 6.56 km/s, the viscosity is less than that of $H_2$ at STP.

*Viscosity of Decomposition Products.*

To model the viscosity of the decomposition products, a very simple approximation is used. We will assume that the decomposition products, which we take to be Si, O, and SiO, are essentially spherical molecules interacting through repulsive potentials and that, for a given ratio of these products, a mean molecular diameter can be defined. To estimate the mean molecular diameter, we will take an average intermolecular repulsive potential $\varphi(r)$, and then define an effective molecular radius $r$, as being half the separation distance at which $\varphi(r) = {}^3/_2kT$, where $k$ is Boltzmann's constant. The volumes of the spherical molecules with this radius make up the excluded volume, which is then used with the bulk volume per molecule in the free volume formulation of viscosity [Hildebrand, 1971], where

$$\eta = B\frac{V_0}{V - V_0}$$

According to van Loef [1979], the value of $B$ for small approximately spherical molecules obeys

$$B = 7.58 \times 10^{-6} M^{1.2}$$

where $M$ is the molecular weight in grams/mole and $B$ is expressed in Pa·s. Assuming that the primary decomposition products are atomic Si and O, we use

$$\varphi(r) = \varepsilon\left[\left(\frac{r_0}{r}\right)^{-2n} - \left(\frac{r_0}{r}\right)^{-n}\right]$$

for the interatomic potential, where $n = 5.9$, $\varepsilon = 9\times10^{-22}$ J , and $r_0 = 3.35$ Å is the radius at which the potential is zero. The choice of $n$ is based on the behavior of argon [Ross, 1980]. The value of $\varepsilon$ is 4 times the mean vaporization energy. The characteristic radius $r_0$ is obtained from the zero point separation distance, $d$, by

$$r_0 = 2^{-1/n} d$$

At present, the parameters for the interatomic potential are averaged from the noble gasses of the periods of O and Si (i.e., Ne and Ar, respectively), based on the results presented by Ross [1980] and tabulations in Harrison [1980]. The excluded volume $V_0$ is related to the actual molecular volume, $V_{mol}$, by [van Loef, 1978]

$$V_0 = 1.89 V_{mol}$$

*Mixing of Viscosity Functions.*

To calculate the actual model viscosity, once the individual end member viscosities are determined, we must have a suitable mixing relation that mimics what is known of real systems. As stated above, we can treat this system as a partially molten system with the polymer being the "solid" and the decomposition products being the "liquid." We could then use the Roscoe's [1952] extension of the Einstein model for the viscosity of a suspension, modified to account for a solid with finite viscosity, with the melt fraction being the fraction of the $SiO_2$ that has decomposed. However, the probability that the polymer will retain more connectivity than might be expected in a solid that has partially melted, we will enforce a more gradual transition in the region of the rheologically critical melt fraction (0.26 in this model). At present, the mixing relation has not been suitably determined. Further work is needed to find the appropriate expression. However, at conditions where a significant fraction of the silica has decomposed, the viscosities of both the decomposition products and the polymeric silica are so low as to make the system essentially inviscid.

## PENETRATION STRENGTH OF AEROGEL

At the terminal portion of the penetration process, when the impacting particle has slowed below the sound speed of the aerogel, the primary source of decelerating force is the strength and elasticity of the aerogel. The particular stress resulting from elastic-plastic deformation and failure is called the penetration strength [Anderson et al., 1986]. A penetrometer was developed (Figure 3) to measure the forces resisting quasistatic penetration. The penetrometer consisted of a micrometer stage that carried the aerogel sample, a cylindrical graphite rod that acted as the penetrator, and a glass fiber that exerted the force driving the penetration of the graphite rod. The flexure of the glass fiber was measured and calibrated to provide a direct measure of the force applied to the penetrator. The force was converted to stress by dividing the applied force by the cross section of the penetrator rod. Penetration tests were conducted on samples provided by F. Hörz of Johnson Space Center and P. Tsou of the Jet Propulsion Laboratory.

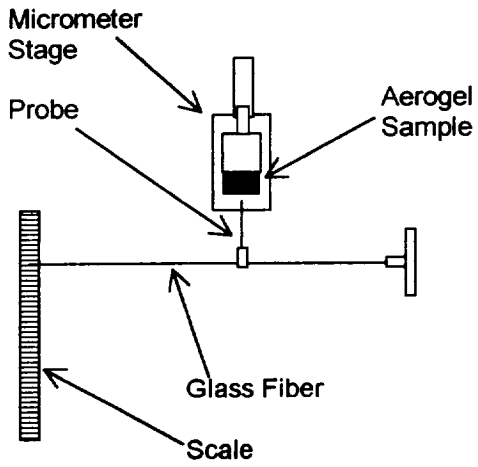


Figure 3. Schematic diagram of penetrometer constructed for this study. The aerogel sample is forced against the probe by the micrometer stage. The resulting flexure of the glass fiber produces a penetrating force on the probe. The fiber was calibrated and the amount of flexure read from the scale. The depth of penetration was determined from the fiber position and the micrometer stage position.

Appendix A presents graphs of the data obtained. Typically, the penetration proceeds by episodes of elastic-plastic deformation of the aerogel, each followed by failure. Visual observation showed that the elastic-plastic deformation occurred in a conical section of the aerogel that became detached from shallower parts of the aerogel at a conical tear or fracture

that grew as penetration progressed. Eventually, the shear strength of the compressed material in the conical section would be exceeded and the probe would break through, initiating another conical tear and the deformation of another conical slug that would be compressed in the same way. In one case, the conical tear became helical and grew steadily as penetration progressed, maintaining a nearly constant resisting force on the penetrator. The track that resulted from this process appears identical to terminal portions of tracks created in aerogel by micrometer-scale particles during laboratory hypervelocity impact studies.

Three quantitative relationships can be derived from the penetrometer data shown in Appendix A. First, the resisting stress resulting from the compression of the conical slug is related to the distance the slug is compressed and the bulk density of the aerogel by

$$\frac{d\sigma}{dx} = \left(4.85\times10^{5}\right)\rho_{00}{}^{1.835}$$

for stress in pascals, distance in meters, and density in kg/m$^3$. Second, although highly variable, the mean applied stress at which the material in the compressed conical slug of material fails is related to the density of the aerogel by

$$\sigma_{fail} = \left(1.28\times10^{4}\right)\rho_{00}$$

for stress in Pa and density in kg/m$^3$. Finally, the mean stress resisting penetration, i.e., the penetration strength, is related to the density of the aerogel by

$$\sigma = \left(2.19\times10^{4}\right)\rho_{00}{}^{1.5}$$

for stress in Pa and density in kg/m$^3$.

There is some uncertainty about the applicability of the foregoing relationships during dynamic penetration. However, the if the application of these relationships is confined to penetration speeds lower than the bulk speed of the aerogel, then these results should be valid. To further understand these samples and the sound speeds, samples used for these measurements have been provided to J. Bass of the University of Illinois at Urbana-Champaign for study using Brilluoin scattering techniques.

## PRELIMINARY MODEL CALCULATIONS

The primary questions faced by mission planners for STARDUST are those associated with successfully sampling dust particles in the 6-7 km/s velocity range. As the shock Hugoniot curves of the densities considered reasonable for the mission are similar, the shock-induced internal energies and hence temperatures are also very similar for a given shock velocity. Since the shock wave in this situation is a bow shock, similar to those produced by supersonic projectiles in a gas, the shock wave will move at the velocity of the duct particle. Hence the choice of aerogel density will have little effect on the temperatures experienced by the particle. However, the duration of exposure to high temperatures can vary considerably.

The primary issue addressed by the calculations performed to date is the minimum mass of aerogel required to reliably stop a particle of a given size and density. Hence, for these

calculations, both viscous drag and ablation have been ignored. A series of calculations was performed for monolithic aerogels and aerogels with various layered density structures. Dust particles with densities of 4.74 $Mg/m^3$ (i.e., troilite) were assumed in order to maximize the penetration depth in the calculations. Five cases are presented here. The total thickness of aerogel in each case is 3.0 cm. Figure 4 shows the different density structures assumed in these calculations. Appendix B contains graphs that show the results for the distance-velocity history for different sizes of particles. Appendix C presents graphs of the pressure-time histories for these calculations. Appendix D presents the results for the temperatures to which the particles are exposed as a function of time.

These preliminary calculations suggest that, to reliably stop a particle in a 3 cm distance, the mean density of aerogel required is related to the particle size and density by

$$\bar{\rho}_0 = 1.085 \times 10^{-4} \rho_p d_p$$

where $\rho_0$ is the aerogel density and $\rho_p$ is the dust particle density, both in $g/cm^3$, and $d_p$ is the dust particle diameter in micrometers. This result is, of course, conservative, since mass loss due to ablation and additional decelerating forces resulting from viscosity effects can be expected to decrease the penetration distance. However, this conservatism allows a margin for error and is needed since a number of issues in the low-velocity behavior of aerogel have yet to be resolved.

All the particles will be exposed to high temperatures. The temperatures will be ~11000 K at the initial impact, and will remain above 5000 K for times periods ranging from ~0.75 μs to 3.5 μs. High aerogel densities are required to minimize time at high temperatures, but this can result in significant shock stresses.

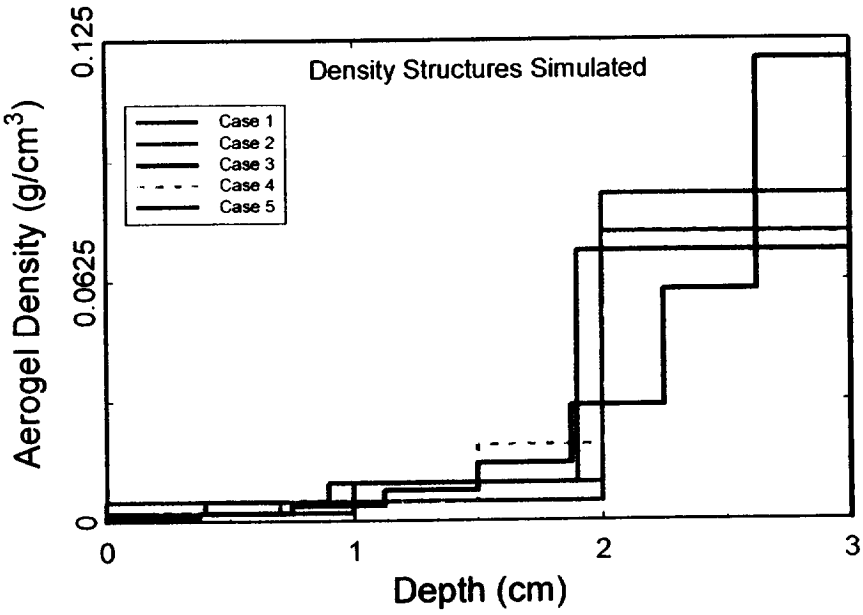


Figure 4. Density structures assumed for the five cases used in the preliminary calculations. The case numbers correspond to those presented in the figures in Appendices B-D.

References:

Anderson, W. W., T. J. Ahrens, A. Gibson, R. Scott, and K. Suzuki, *J. Geophys. Res.*, *101*, 21137-21150, 1996.

Arzi, A. A., *Tectonophysics, 44*, 173-184, 1978.

Harrison, W. A., *Electronic Structure and the Properties of Solids*, Dover, 586 pp., 1980.

Hildebrand, J. H., *Science, 174*, 490, 1971.

Holmes, N. C., in *High Pressure Science and Technology - 1993*, 153-156, 1994.

Holmes, N. C., H. B. Radousky, M. J. Moss, W. J. Nellis, and S. Henning, *Appl. Phys. Lett., 45*, 626-628, 1984.

Holmes, N. C., and E. F. See, in *Shock Compression of Condensed Matter 1991*, 91-94, 1992.

Rabie, R., and J. J. Dick, in *Shock Compression of Condensed Matter 1991*, 87-90, 1992.

Roscoe, R., *Br. J. Appl. Phys., 3*, 267-269, 1952.

Ross, M., *J. Chem. Phys., 73*, 4445-4450, 1980.

Simakov, G. V., and R. F. Trunin, *Izv. Earth Physics, 26*, 952-956, 1990.

Van Loef, J. J., *J. Chem. Soc. Faraday Trans. I, 75*, 2061-2066, 1979.

Vildanov, V. G., M. M. Gorshkov, V. M. Slobodenjukov, and E. H. Rushkovan, in *Shock Compression in Condensed Matter - 1995*, 121-124, 1996.

Weast, R. C., *CRC Handbook of Chemistry and Physics*, 56th ed., CRC Press., 1975.

Weiss, W., *J. Am. Ceramic Soc., 67*, 213-222, 1984.

## Appendix A.

The following figures present the experimental data of applied stress versus penetration depth for penetrometer tests with four densities of aerogel. The penetration behavior can be seen in each case to increase monotonically, often with small failures. In cases where substantial penetration was achieved, one or more episodes of sudden failure, accompanied by large increases in penetration depth and decreases in applied stress. In all cases, large hysteresis was observed on unloading, indicating permanent densification of the aerogel in the penetration process, even when a significant failure event did not occur.

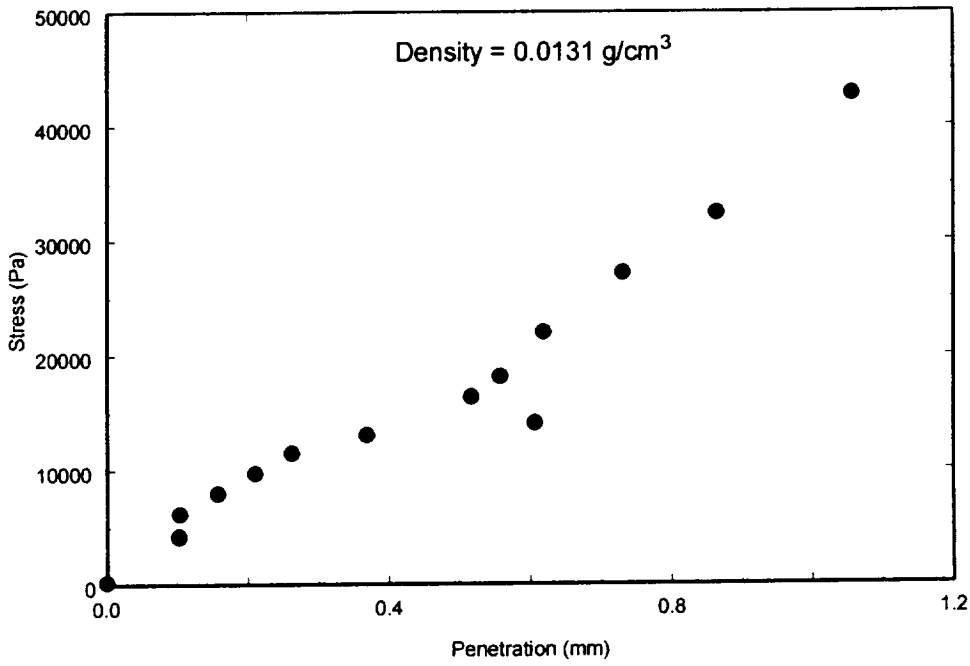

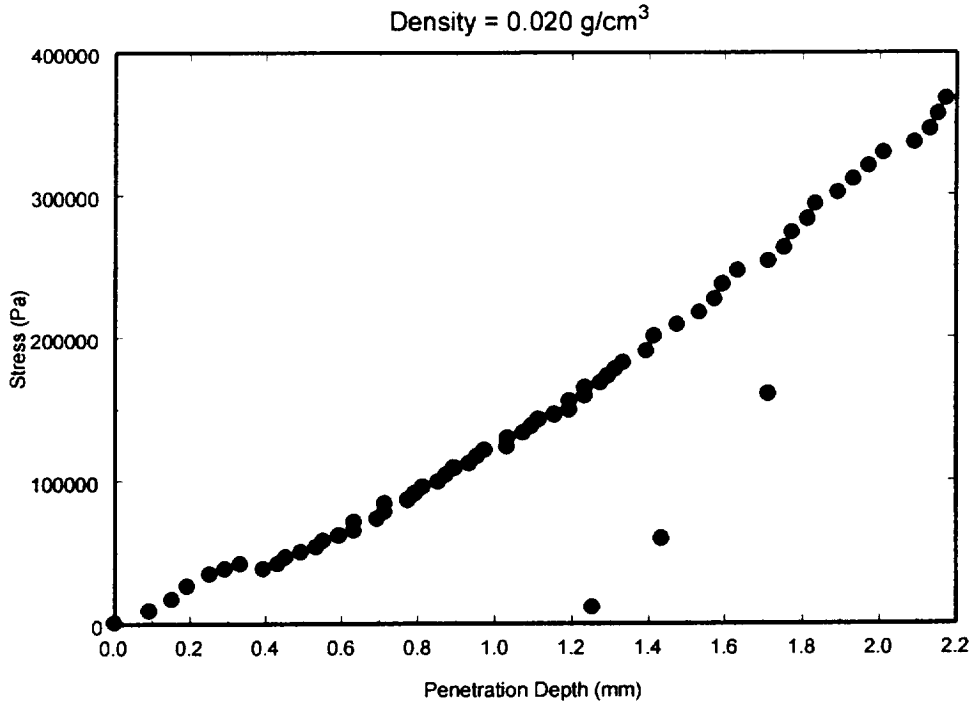
Density = 0.020 g/cm3
Stress (Pa)
400000
300000
200000
100000
0
0.0
0.2
0.4
0.6
0.8
1.0
1.2
1.4
1.6
1.8
2.0
2.2
Penetration Depth (mm)

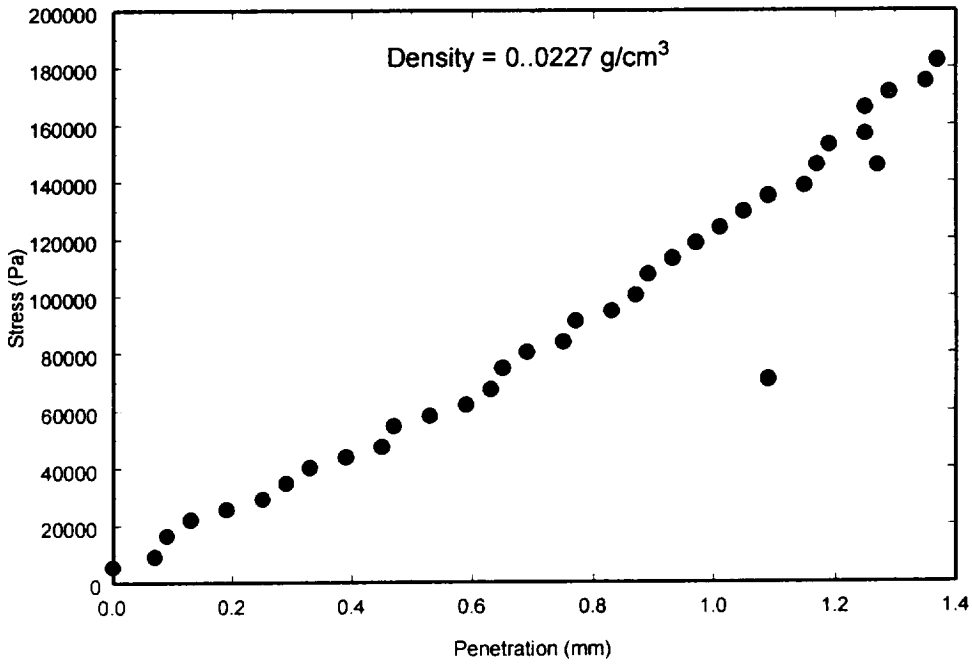
Density = 0..0227 g/cm3
Stress (Pa)
200000
180000
160000
140000
120000
100000
80000
60000
40000
20000
0
0.0
0.2
0.4
0.6
0.8
1.0
1.2
1.4
Penetration (mm)

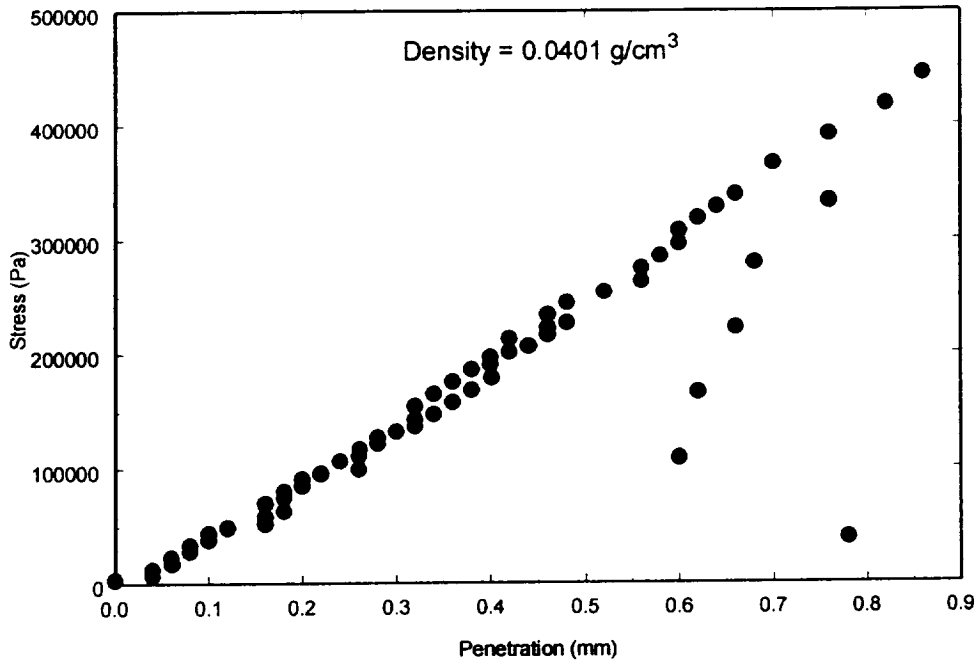
Density = 0.0401 g/cm3
Stress (Pa)
500000
400000
300000
200000
100000
0
0.0
0.1
0.2
0.3
0.4
0.5
0.6
0.7
0.8
0.9
Penetration (mm)

## Appendix B.

Velocity versus position for the preliminary calculations discussed in the text. The case numbers refer to the aerogel density distributions presented in figure 4 in the text.

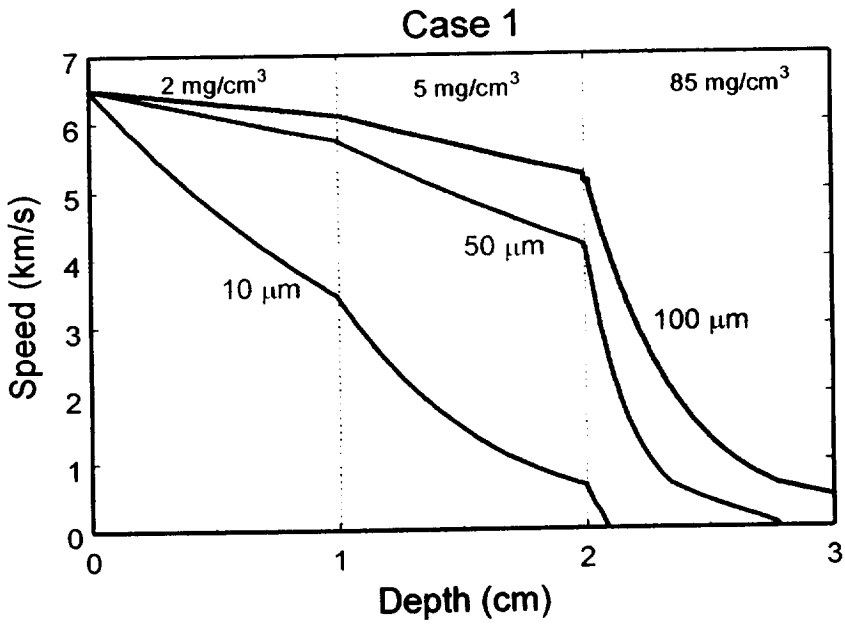

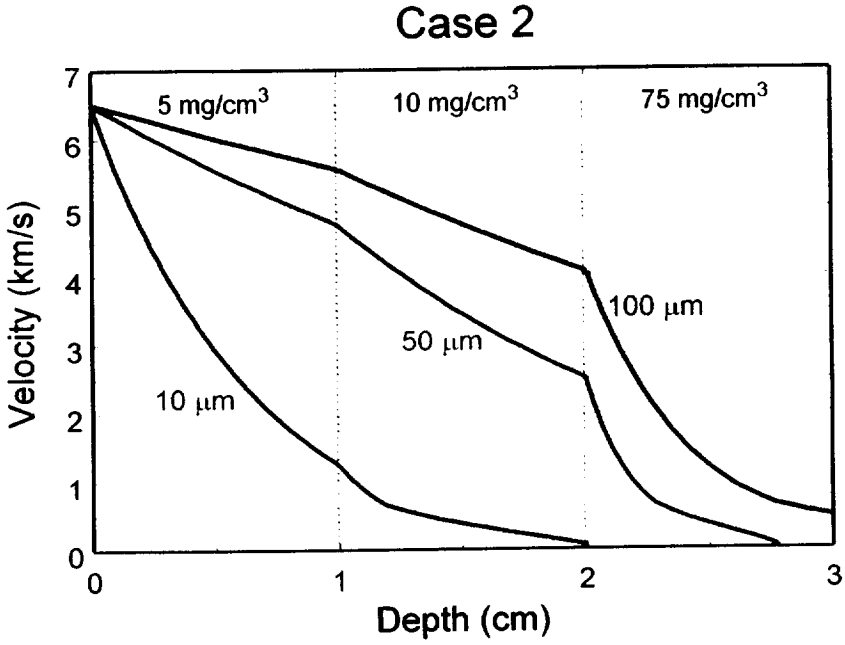
Case 2
5 mg/cm3
10 mg/cm3
75 mg/cm3
100 μm
50 μm
10 μm
Velocity (km/s)
Depth (cm)
0
1
2
3
4
5
6
7

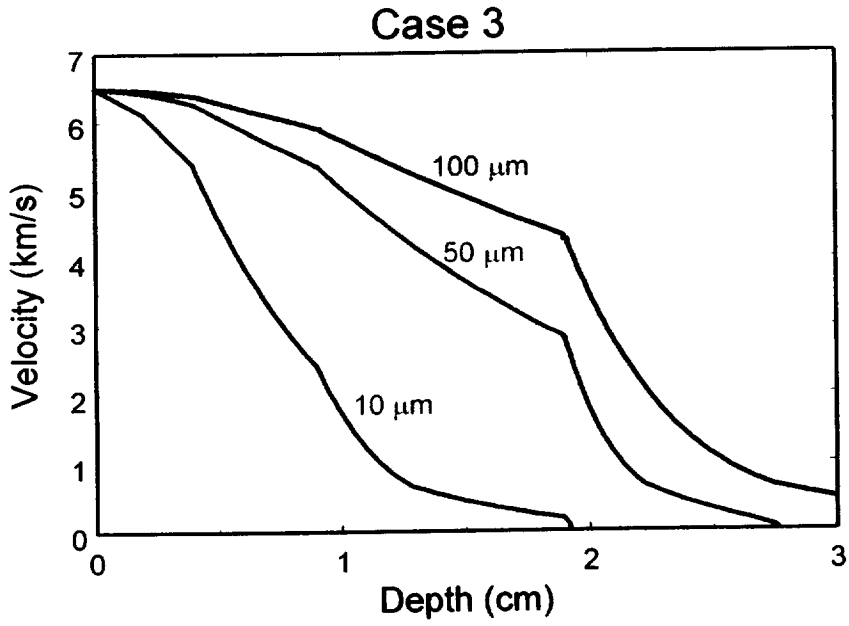
Case 3
100 μm
50 μm
10 μm
Velocity (km/s)
Depth (cm)
0
1
2
3
4
5
6
7

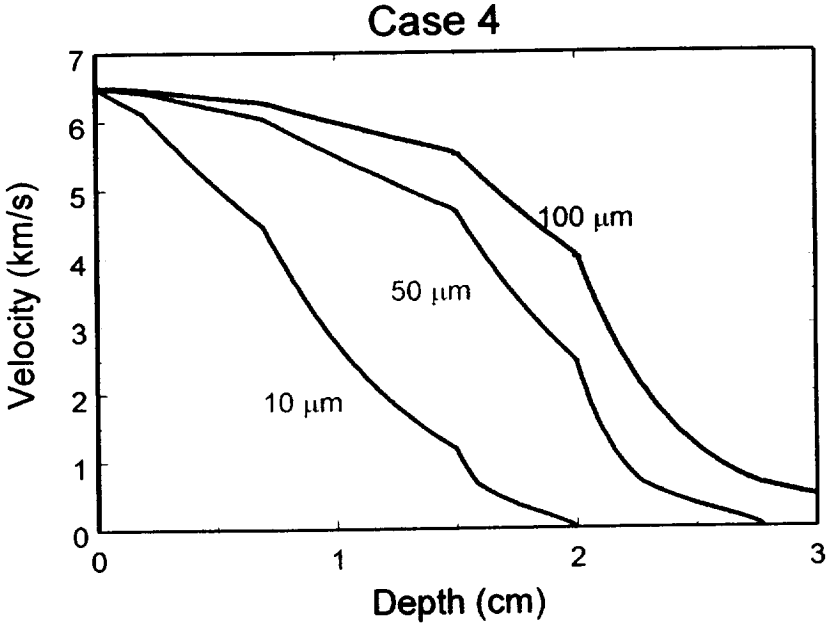
Case 4
Velocity (km/s)
Depth (cm)
100 μm
50 μm
10 μm
0
1
2
3
4
5
6
7

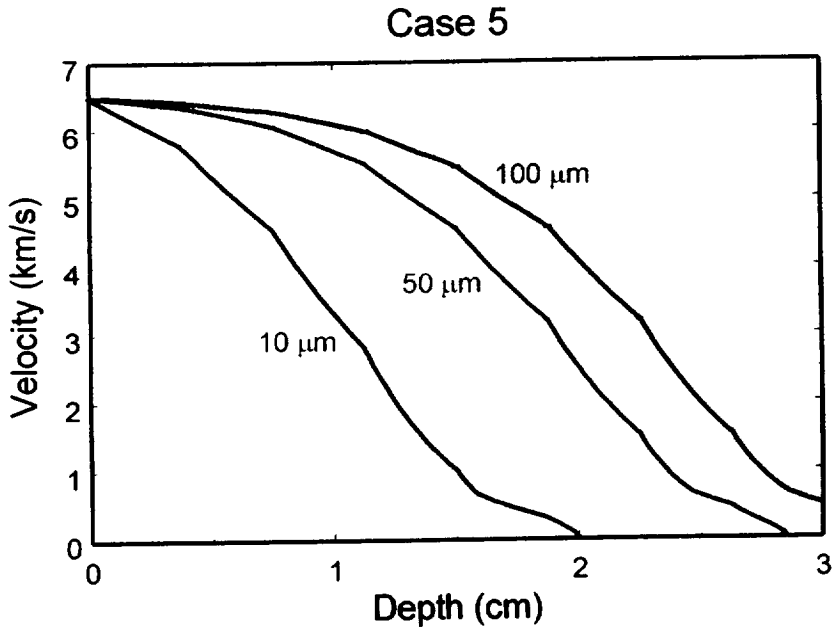
Case 5
Velocity (km/s)
Depth (cm)
100 μm
50 μm
10 μm
0
1
2
3
4
5
6
7

## Appendix C.

Pressure-time histories for particles from the preliminary calculations discussed in the text. The spikes occur at times when the particles encounter density discontinuities in the aerogel. The case numbers refer to the aerogel density distributions presented in figure 4 in the text.

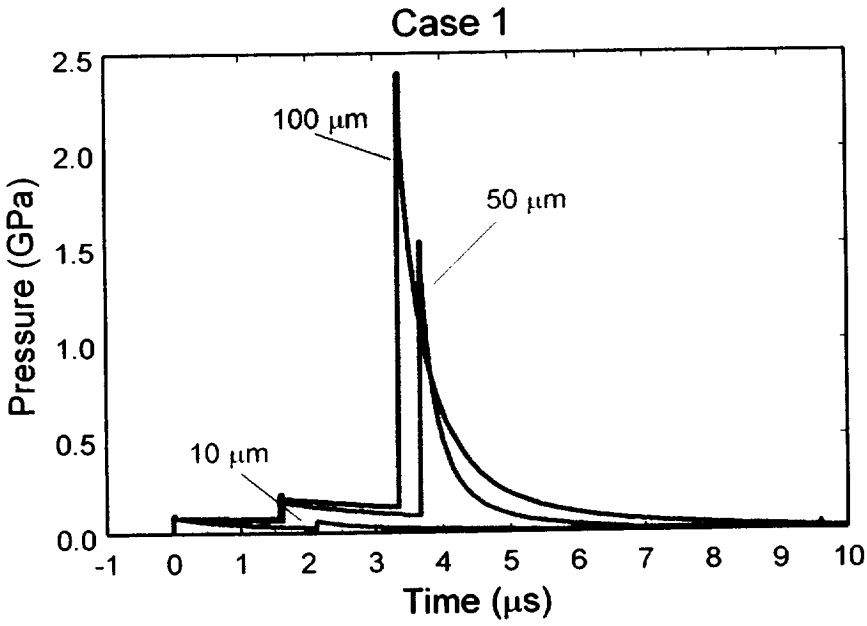

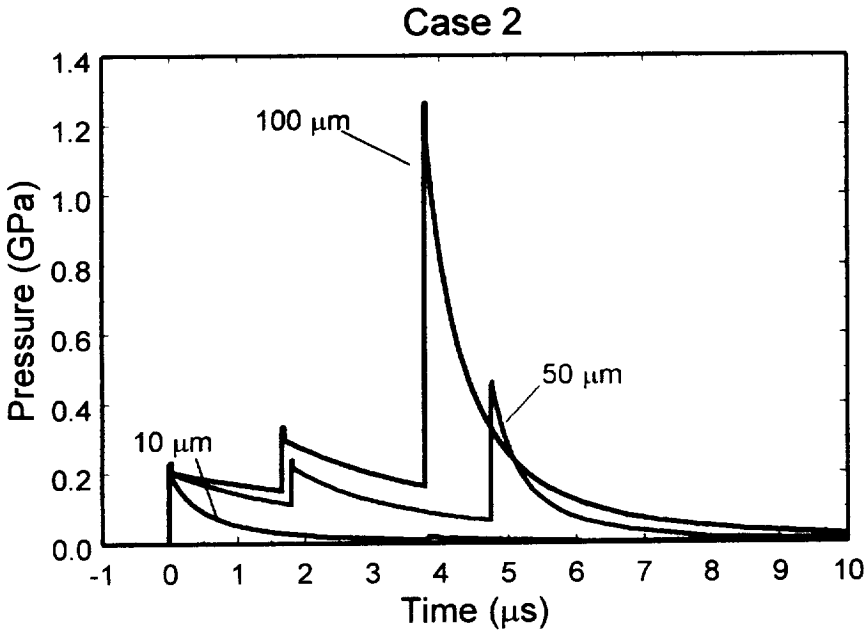
Case 2
Pressure (GPa)
Time (μs)
100 μm
50 μm
10 μm
1.4
1.2
1.0
0.8
0.6
0.4
0.2
0.0
-1
0
1
2
3
4
5
6
7
8
9
10

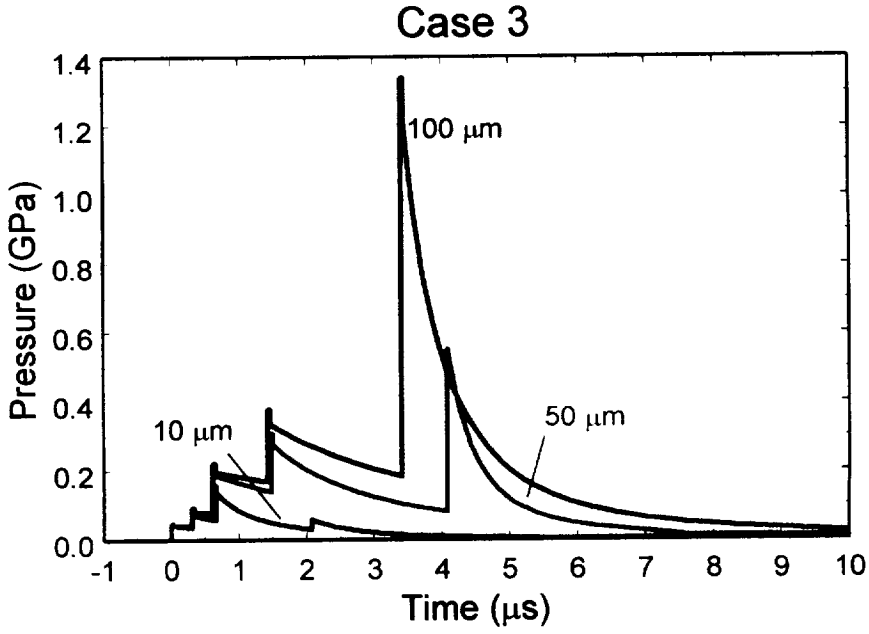
Case 3
Pressure (GPa)
Time (μs)
100 μm
50 μm
10 μm
1.4
1.2
1.0
0.8
0.6
0.4
0.2
0.0
-1
0
1
2
3
4
5
6
7
8
9
10

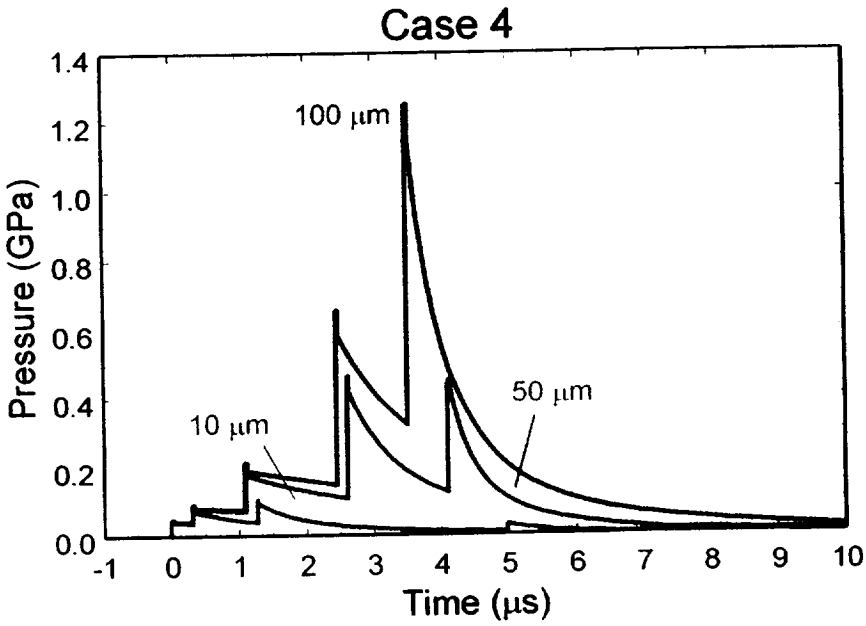
Case 4
Pressure (GPa)
Time (μs)
100 μm
50 μm
10 μm
1.4
1.2
1.0
0.8
0.6
0.4
0.2
0.0
-1
0
1
2
3
4
5
6
7
8
9
10

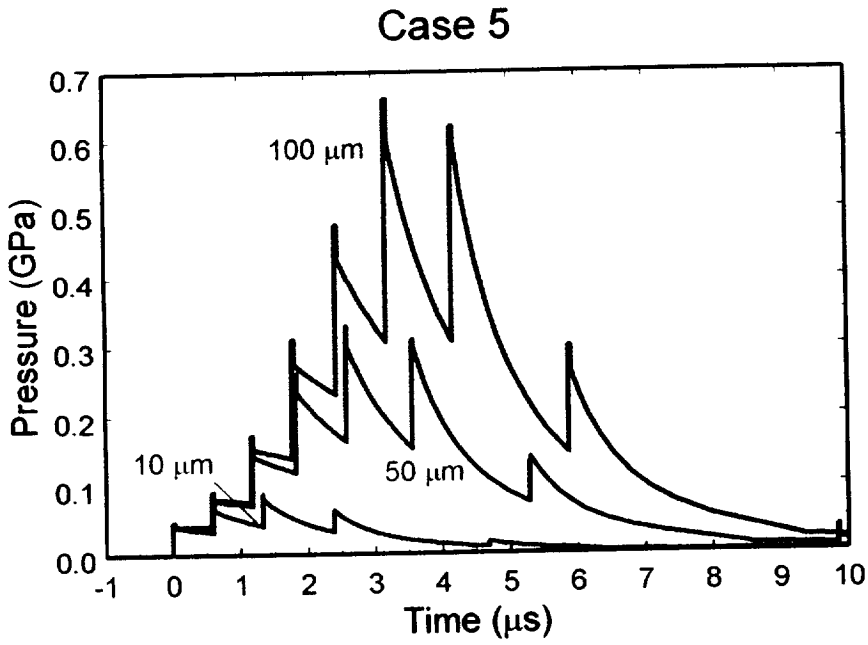
Case 5
Pressure (GPa)
Time (μs)
100 μm
50 μm
10 μm
0.7
0.6
0.5
0.4
0.3
0.2
0.1
0.0
-1
0
1
2
3
4
5
6
7
8
9
10

## Appendix D.

Temperature histories experienced by particles in the preliminary calculations. The temperatures are those of the shocked aerogel flowing past the particle at the relevant times. The spikes occur at times when density interfaces are encountered.

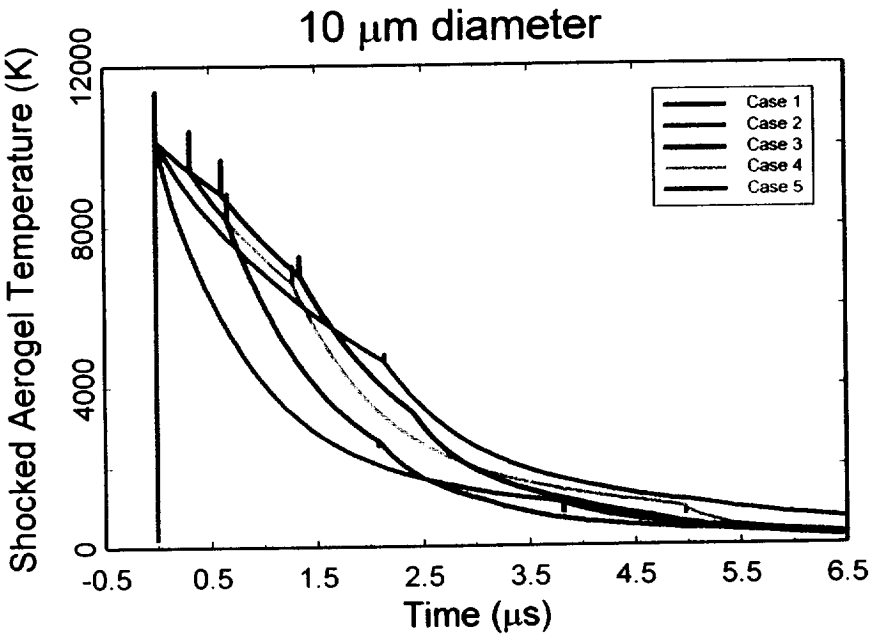

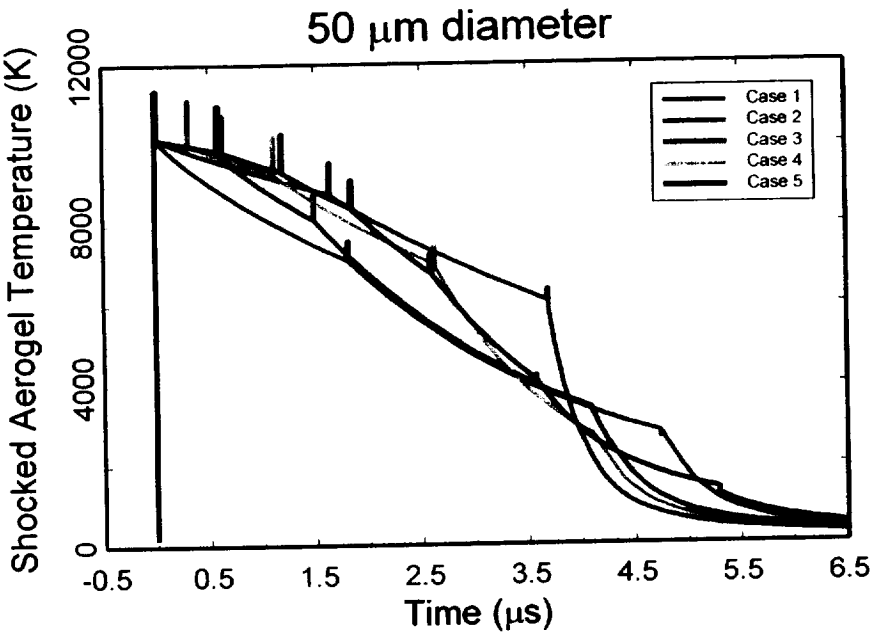
50 μm diameter
Shocked Aerogel Temperature (K)
0
4000
8000
12000
-0.5
0.5
1.5
2.5
3.5
4.5
5.5
6.5
Time (μs)
Case 1
Case 2
Case 3
Case 4
Case 5